STATE OF OREGON
DEPARTMENT OF GEOLOGY AND MINERAL INDUSTRIES
VICKI S. McCONNELL, STATE GEOLOGIST

Geologic Map of the Hawks Valley - Lone Mountain Region, Harney County, Oregon

2011

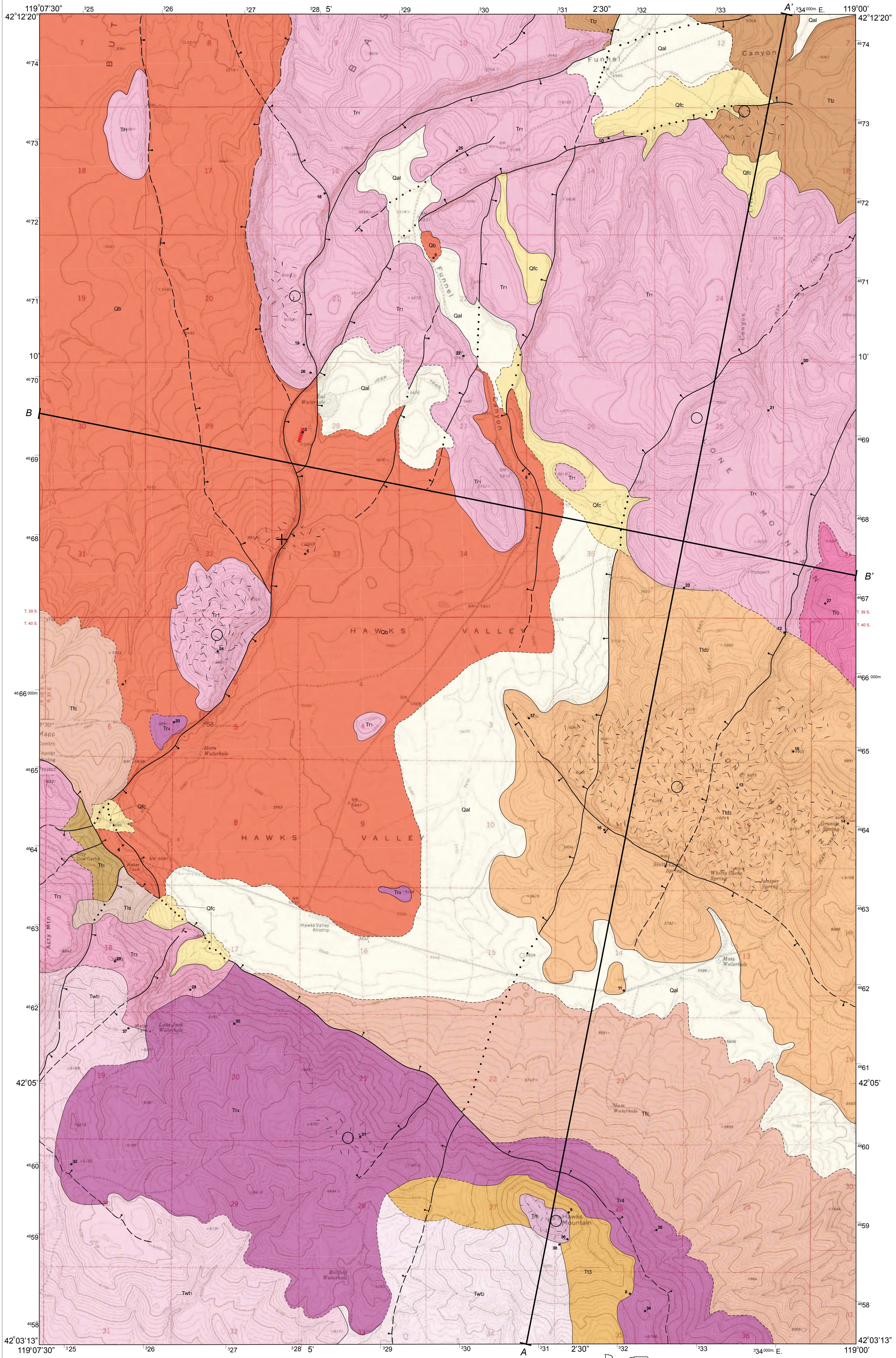

Base map by U.S. Geological Survey
Control by USGS and USC&GS
Topography by photogrammetric methods from aerial photographs taken 1971. Field checked 1971
Projection and 10,000-foot grid ticks: Oregon coordinate system, south zone (Lambert conformal conic)
1000-meter Univrsal Transverse Mercator grid ticks, zone 11, shown in black. 1927 North American datum
Fine red dashed lines indicate selected fence lines

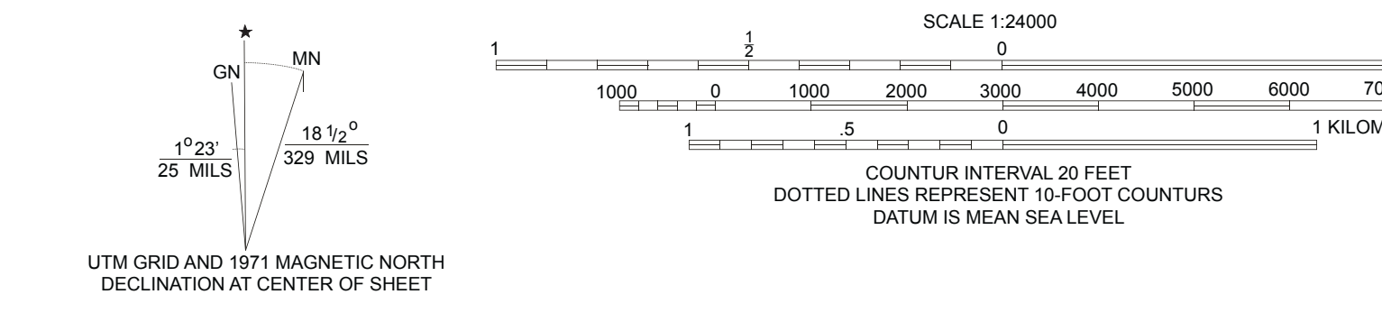

UTM GRID AND 1971 MAGNETIC NORTH DECLINATION AT CENTER OF SHEET

COUNTUR INTERVAL 20 FEET
DOTTED LINES REPRESENT 10-FOOT COUNTURS
DATUM IS MEAN SEA LEVEL

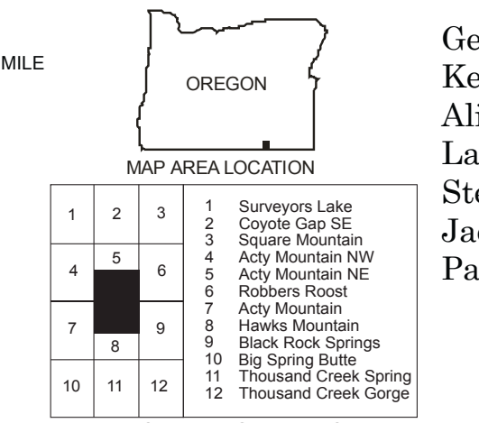

MAP AREA LOCATION

1 Surveyors Lake
2 Coyote Gap SE
3 Square Mountain
4 Acty Mountain NW
5 Acty Mountain NE
6 Robbers Roost
7 Acty Mountain
8 Hawks Mountain
9 Black Rock Springs
10 Big Spring Butte
11 Thousand Creek Spring
12 Thousand Creek Gorge

7.5' QUADRANGLE NAMES

Geology by :
Kelly C. McHugh, William K. Hart - 2010 (EdMap Project)
Alicja Wypych, Kaleb C. Scarberry, Kelly C. McHugh,
Laura J. Flores, William K. Hart - 2009 (EdMap Project)
Stephen A. Pasquale, Matthew E. Brueseke,
Jacob E. Knight, William K. Hart - 2004
Paul W. Legge -1985

GEOLOGIC CROSS SECTIONS

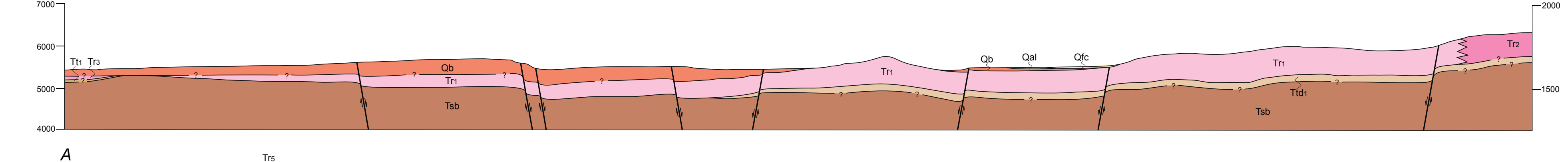

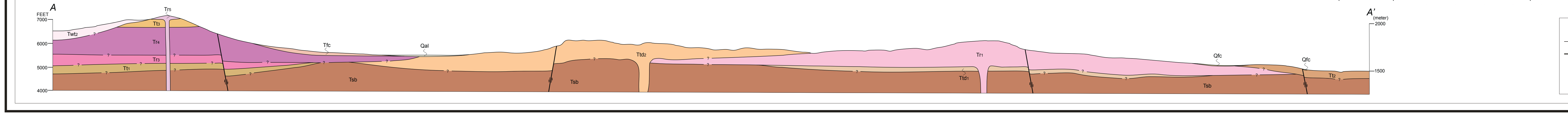

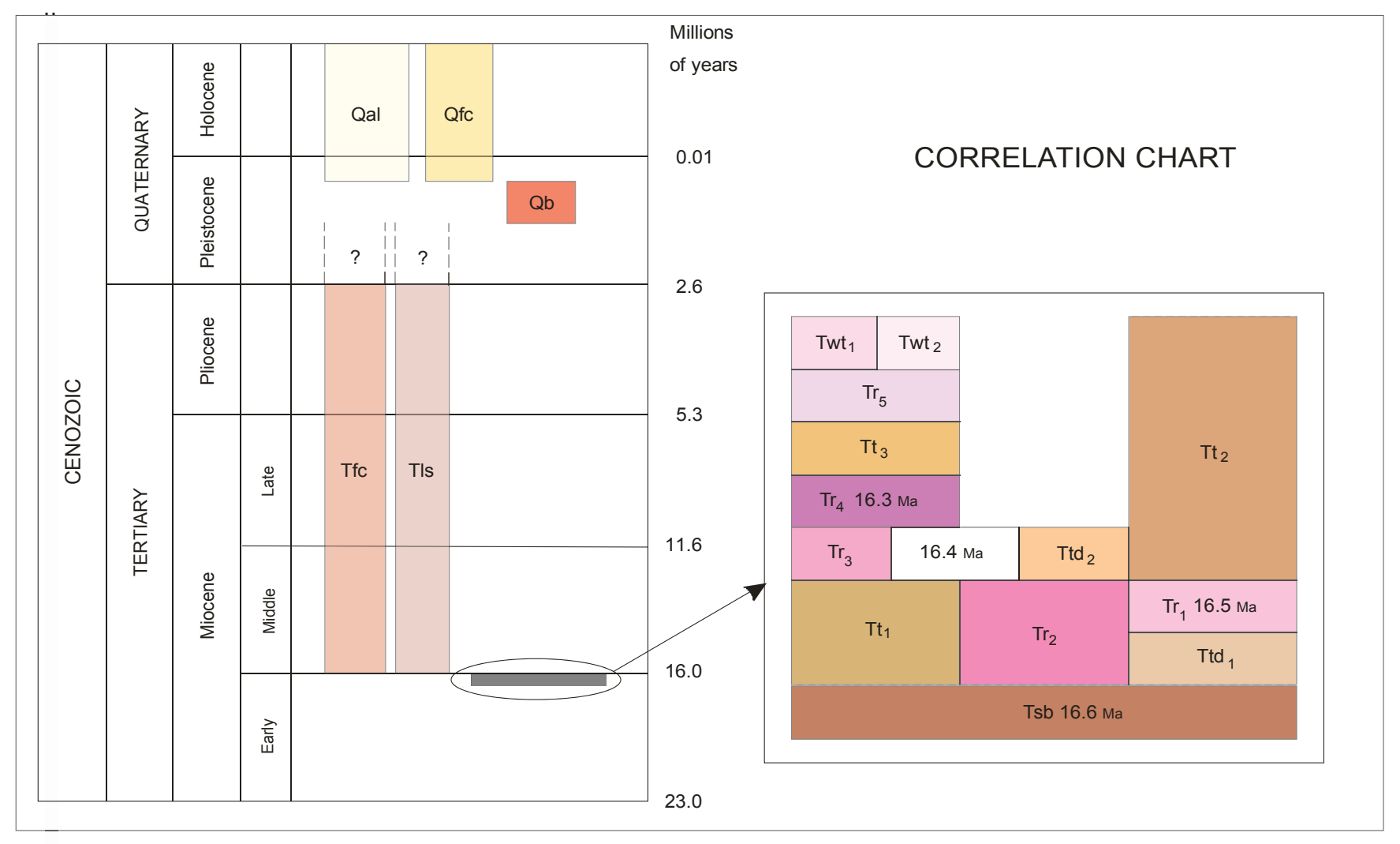

EXPLANATION OF MAP UNITS

Qal — **Alluvium (Holocene and Pleistocene)** – Unconsolidated, moderately well sorted sand and silt deposits along modern stream flood plains and in small paleodepressions.

Qfc — **Colluvial and alluvial fan deposits (Holocene and Pleistocene)** – Mainly alluvial fan and slope deposits of unconsolidated coarse gravels and sands. Colluvial deposits include primarily scree and talus. Gravel, scree and talus contain rhyolitic and basaltic material.

Qb — **Basalt flows (Pleistocene)** – Qb is exposed throughout Hawks Valley, in southern Funnel Canyon, and across the northwestern portion of map area and is best exposed in the northeast trending fault scarp defining the western edge of Hawks Valley where multiple compound pahoehoe flow units ranging in thickness from 5-15 m are observed. Local thinner, clastogenic flows and agglutinate are observed proximal to a remnant cone bisected by the NE-trending fault and an eruptive fissure along the base of the fault. A minimum aggregate thickness of 90 m is estimated. The basalt is holocrystalline with plagioclase > augite > olivine > oxides and often phenocrysts and glomerocrysts of olivine and plagioclase. Qb is characteristically diktytaxitic and subophitic with intergranular oxide. The petrography and chemistry of this entire basalt package corresponds to the regionally important low-K, high-alumina olivine tholeiite (HAOT) basalt type defined by Hart et al. (1984). Two whole-rock K-Ar age determinations (0.47 ± 0.23 Ma, fault scarp and 0.81 ± 0.25 Ma, Funnel Canyon) constrain this unit to the Pleistocene.

Tfc — **Colluvial and alluvial fan deposits (Pliocene and Miocene)** – Mainly alluvial fan and slope deposits of unconsolidated coarse gravels and sands. Colluvial deposits include primarily scree and talus. Gravel, scree and talus contain rhyolitic material. Exposed prominently along southern margin of Hawks Valley adjacent to Hawks Mountain.

Tls — **Landslide deposits (Pliocene and Miocene)** – Poorly sorted talus consisting of rhyolitic gravel, sand and silt.

Tsb — **Steens Basalt (Miocene)** – The Steens Basalt is widespread across southern Oregon and adjacent regions with eruptive localities concentrated in but not limited to the Steens-Pueblo Mountains, and thick stratigraphic sections prominently exposed to the west and east of the map area (e.g., Carlson and Hart, 1987). Tsb is not exposed in the HVLM, but units Tr_2 and Tt_2 appear to on-lap Tsb to the E-NE of the map area, and units presumably correlative to Twt_1 and Twt_2 overlie the Tsb to the east and south of the map area. Using the same Ar calculation parameters employed in this study an age of 16.6 ± 0.1 Ma is suggested for the Tsb that likely underlies the HVLM (e.g., Henry et al., 2006; Jarboe et al., 2010 and references therein).

Silicic Units of the Acty Mountain – Hawks Mountain Region

Twt_1 — **Welded ash-flow tuff (Miocene)** – Twt_1 is widely exposed to the west, south and southwest of Acty Mountain extending for at least 20-25 km to Oregon/Nevada Highway 291/140 and beyond, reaching local thicknesses in excess of 25 meters. Isolated ~5 m thick patches of Twt_1 are exposed on top of the NE-trending Hawks Valley fault scarp, locally overlying Tr_1, where the unit is weathered to a deep red. Twt_1 appears to on-lap the lava flow material comprising the high regions from Hawks Mountain to Acty Mountain, thus may represent among the youngest silicic materials in the map area. Fresh surfaces are gray to pink with ovoid to flattened black fiamme that when weathered provide a "swiss cheese" appearance. Locally this unit displays prominent lithophysal zones. Minor crystals of sanidine and oxides and sparse intermediate to mafic lithic fragments are set in an intensely welded glassy groundmass displaying secondary flowage with aligned and variably devitrified fiamme. The wide inferred distribution, intense welding, and rheomorphic features suggest emplacement as a high-temperature ash-flow sheet(s). The aerial extent, petrography, and chemistry suggest that Twt_1 is correlative with the Idaho Canyon Tuff/Oregon Canyon Tuff (Walker and McLeod, 1991; Rytuba and McKee, 1984; Green, 1984; Colgan et al., 2006; Henry et al., 2006; Lerch et al., 2008; C. Henry and M. Coble, personal communication, 2010). Based on this link and using the same Ar calculation parameters employed in this study, an age of 16.3 ± 0.2 Ma is inferred for Twt_1 (above and Jarboe et al., 2010).

Twt_2 — **Welded ash-flow tuff (Miocene)** – Twt_2 appears to on-lap the lava flow material comprising the southwestern side of Hawks Mountain with more extensive exposures extending to the south of the map area. Clear stratigraphic relationships between Twt_1 and Twt_2 are not observed within or adjacent to the map area. Within the map area outcrops of this unit are up to 20 m thick and weather into spires. The unit is readily distinguished from Twt_1 by being crystal rich with 2 to 4 mm feldspar set in a dark gray to black dense, fine-grained matrix. Tan pumice up to 1 cm in size also is common. In thin section sanidine, plagioclase, biotite, and pyroxene phenocrysts are observed in a glassy, devitrifying matrix. Feldspars are up to 3 mm in size and commonly are step-zoned or display partially resorbed edges and a cellular texture. Biotite and pyroxenes occur in minor amounts with pyroxene commonly preserving compositional zonation. Similar to Twt_1, a source well to the south of the map area is suggested (Walker and McLeod, 1991; Green, 1984). The field relations also are consistent with an age similar to that inferred for Twt_1, or possibly even a more direct link with these two units representing different flow units of the Idaho Canyon Tuff.

Tr_5 — **Rhyolite (Miocene)** – Tr_5 (Hawks Mountain rhyolite) is restricted to the present-day summit area of Hawks Mountain where it conformably overlies Tt_3. This unit typically is platy and flow banded with a gray to purple matrix hosting feldspar phenocrysts and visible biotite. Tr_5 is difficult to distinguish from Tr_4, but stratigraphic relationships require formal distinction. In thin section the rhyolite displays a fine-grained feldspar dominated, hypocrystalline groundmass with plagioclase and sanidine phenocrysts up to 2.5 mm and scattered biotite and oxide. Although no source vent has been established, the outcrop pattern is consistent with a source proximal to Hawks Mountain.

Tt_3 — **Trachyte (Miocene)** – Tt_3 (Hawks Mountain trachyte) is observed only near the top of Hawks Mountain where it is no thicker than 150 m and stratigraphically overlies Tr_4. The upper portion of the trachyte weathers into plates that display a very fine grained gray to black matrix containing clinopyroxene and orthopyroxene phenocrysts up to 2 mm and abundant plagioclase phenocrysts up to 5 mm. In thin section these phenocrysts and glomeroporphyritic clusters of plagioclase and pyroxene are set in a hypocrystalline matrix containing numerous flow aligned plagioclase laths providing a trachytic texture. Although no source vent has been firmly established, the outcrop pattern is consistent with a source proximal to or just to the southeast of Hawks Mountain.

Tr_4 — **Rhyolite (Miocene)** – Tr_4 (Saddle Dome rhyolite) completely surrounds Hawks Mountain extending as far southeast as Lone Juniper, and is continuously exposed to the southwest of the main NW-trending Hawks Valley fault scarp between Acty Mountain and Hawks Mountain. The Saddle Dome rhyolite represents multiple flow units with an estimated aggregate thickness of at least 300 m, displays a characteristic gray to purple color with visible dark flow banding, and locally preserves thick upper vitrophyre and frothy, pumiceous flow top. Distinct large flow lobes are discerned and point to a possible central eruptive locality between Acty and Hawks Mountains. In thin section this rhyolite displays fine-grained feldspar dominated or devitrified glass matrix hosting crystals of predominantly plagioclase, anorthoclase, and sanidine up to 4.5 mm in size. Thus, while the unit has a porphyritic texture, in some samples there can be as much as 95% matrix and only 5% crystals. Iron-titanium oxides, biotite, and clinopyroxene are ubiquitous microphenocrysts. Feldspars from a Tr_4 vitrophyre yield an Ar-Ar age of 16.33 ± 0.17 Ma.

Tr_3 — **Rhyolite (Miocene)** – Tr_3 (Acty Mountain rhyolite) is found only proximal to Acty Mountain achieving an estimated aggregate thickness of 180 m. Individual exposures up to 25 m thick exhibiting 5-10° S-SE dips away from the Acty Mountain summit region suggest an eruptive locality just to the west of the map area. This unit displays well developed flow banding, typically is pervasively oxidized with a thick weathering rind, and locally preserves zones of vitrophyre. Fresh surfaces expose a light gray to light purple hypocrystalline matrix with feldspar crystals. In thin section Tr_3 is porphyritic with cryptocrystalline to glassy groundmass showing contorted flow banding. Phenocrysts include sanidine (up to 3 mm), fayalitic olivine (up to 1 mm), clinopyroxene, and biotite. Feldspars from a Tr_3 vitrophyre yield an Ar-Ar age of 16.39 ± 0.17 Ma. While this age is indistinguishable from that determined for the Saddle Dome rhyolite, it is in agreement with field observations that place Tr_4 stratigraphically above Tr_3.

Tt_1 — **Trachyte (Miocene)** – Tt_1 (Bald Mountain trachyte) is prominently exposed to the west of the map area along the northern flank of Bald Mountain and projects into the map area in the Acty Mountain region where it is up to 60 m thick and observed to uncomfortably underlie the Acty Mountain rhyolite (Tr_3). In hand sample the rock is gray to black, massive and fine-grained, with identifiable flow banding accentuated by weathering. Microphenocrysts of plagioclase, orthopyroxene, clinopyroxene and iron-titanium oxide are most obvious in thin section but visible in hand sample.

Silicic Units of the Funnel Canyon Region

Tt_2 — **Trachyte (Miocene)** – Tt_2 (Basque Hills trachyte) crops out in the northeastern portion of the map area in and adjacent to Funnel Canyon, along the southeastern flank of Lone Mountain, and well to the east of the map area along the western flank of the Pueblo Mountains, and is estimated to possess a minimum thickness of 15 m. Along the western edge of Funnel Canyon Tt_2 appears to overlie the Funnel Canyon rhyolite (Tr_1). Two possible vent areas are inferred; in the northeastern corner of the map area and outside the map area at the northeastern terminus of Funnel Canyon. Outcrops are typically massive with flattened vesicles at the top to platy at the base. In hand sample the unit is black and very fine grained with prominent feldspar crystals. In thin section Tt_2 displays a very fine pilotaxitic feldspar-glass matrix with plagioclase, orthopyroxene, and clinopyroxene. Plagioclase crystals are up to 5 mm, resorbed to skeletal. This unit is readily distinguished from most others by the lack of alkali feldspar phenocrysts and by pilotaxitic plagioclase aligned with flattened vesicles. A whole-rock aliquot of this material yielded a K-Ar age of 16.25 ± 0.26 Ma.

Tr_1 — **Rhyolite (Miocene)** – Tr_1 (Funnel Canyon rhyolite) crops out extensively along the northwest flank of Lone Mountain and dominates the exposures throughout the southern portion of Funnel Canyon where numerous N-NE trending fault scarps reveal individual flow unit thicknesses of at least 30 m and an aggregate thickness of no less than 300 m. The upper flow margins are characterized by porphyritic vitrophyre. This unit is light to dark gray on fresh surface with some color variations of pink and tan, and weathers red to black. Outcrops and hand samples display pronounced wavy to contorted flow banding. The eastern contact relationships with Lone Mountain units Tr_2 and Ttd_2 are stratigraphically ambiguous. Two possible vent localities are observed in Funnel Canyon where brecciated oxidized vitrophyre caps intensely contorted, vertically flow banded rhyolite. Two additional vents are identified as domes along the southwestern edge of the main Tr_1 exposure (Hill 6089/90) and on the upthrown side of the young Hawks Valley fault ("Scarp" Dome). In thin section Tr_1 is porphyritic to glomeroporphyritic with a cryptocrystalline to fresh glassy matrix. Flow banding is evident in alternating bands of decreased glass and increased broken crystals. Phenocrysts include sanidine, plagioclase, orthopyroxene, biotite, and clinopyroxene. Feldspars are subhedral to anhedral often displaying disequilibrium features and are up 3.5 mm in length. The smaller mafic crystals often are altered to chlorite. At least three chemically distinct Tr_1 flow units are identified, but these are indistinguishable in field appearance hence are not indicated on the map. Feldspars from a Tr_1 vitrophyre yield an Ar-Ar age of 16.51 ± 0.25 Ma.

Ttd_1 — **Trachydacite (Miocene)** – Ttd_1 (Funnel Canyon trachydacite) has been identified in only one location within the map area, along the southern-most main fault bounding the eastern side of Funnel Canyon. Here Ttd_1 conformably underlies the Funnel Canyon rhyolite. Additional exposures and a possible Ttd_1 vent locality are observed just east of the northeastern portion of the map area. Based on these exposures a minimum unit thickness of 60 m is estimated. Ttd_1 is gray on fresh surface and weathers to yellow-brown. Flow banding is visible in outcrop and in thin section where it is accentuated by alignment of crystals. The unit is porphyritic with a cryptocrystalline to glassy matrix and anhedral phenocrysts (2-5 mm) of sanidine, plagioclase, clinopyroxene and biotite.

Silicic Units of Lone Mountain

Ttd_2 — **Trachydacite (Miocene)** – Ttd_2 (Lone Mountain trachydacite) is exposed in the southwestern portion of Lone Mountain and is interpreted as remnants of a large silicic dome core with surrounding outflow. The aggregate unit thickness is estimated to be up to 330 meters. The dome core itself is extensively exfoliated and heavily jointed and displays distinctive weathering patterns of rounded pinnacles and jagged forms not observed elsewhere the map area. Ttd_2 is light gray on fresh surface and weathers from white to yellow-brown. Flows emanating from the core have a darker matrix, ranging from dark gray to black, weather to a deep red color, and weather more sharply than the exfoliated core. Prominent flow features are visible on outcrop scale with individual flow units up to 20-50 m thick. Upper and lower flow vitrophyres are common. Some vertical to near-vertical flow patterns are locally observed that may represent feeder localities. These features vary from small discontinuous dikes (5 m high, 30 m in length along the margin of the dome) to a volcanic plug (25 m high, 20 m in length in the central part of the dome). The distinction between the dome core and flows emanating from this core are based on the presence or absence of flow features, rock color and weathering pattern. In thin section Ttd_2 displays slight flow banding and a cryptocrystalline to glassy matrix. with phenocrysts of anorthoclase, sanidine, plagioclase, biotite, and clinopyroxene. Most crystals are anhedral, and anorthoclase and sanidine range up to 4 mm and plagioclase up to 5.5 mm in length. The biotite and clinopyroxene are altered to chlorite/clay/oxide. Feldspars from two separate glassy Ttd_2 samples yield Ar-Ar ages of 16.40 ± 0.19 and 16.46 ± 0.21 Ma and a whole-rock K-Ar determination yields an age of 16.38 ± 0.26 Ma.

Tr_2 — **Rhyolite (Miocene)** – Tr_2 (Lone Mountain rhyolite) underlies Ttd_2 in the central and eastern portions of Lone Mountain extending well off of the map area to the north and northeast. Flow lobes/fronts of the Funnel Canyon rhyolite (Tr_1) and the Lone Mountain rhyolite are juxtaposed in undetermined stratigraphic contexts along the north-northwest flank of Lone Mountain. Exposures in stream cuts indicate a minimum thickness for Tr_2 of 50 m. Both upper and lower flow vitrophyres are observed and frothy, pumiceous upper flow material is locally preserved. This unit is light to dark gray with hues of pink and blue on freshly exposed surfaces and is visibly flow banded. Weathered surfaces are tan with clay filling in cavities. In thin section Tr_2 is sparsely porphyritic with a cryptocrystalline, banded spherulitic groundmass. Phenocrysts include sanidine, plagioclase, clinopyroxene, and biotite. Feldspars display disequilibrium textures, with sanidine up to 5 mm and plagioclase up to 1.25 mm in length. Field distinction between Tr_2 and Tr_1 is difficult, but chemical differences are notable. Tr_2 is distinguished from other silicic units by a combination of being matrix-dominated (>80%) and devoid of anorthoclase.

OVERVIEW AND GEOLOGIC SETTING

The Hawks Valley-Lone Mountain area (HVLM) of southeastern Oregon exemplifies regional relationships between extensional tectonics and magmatism. Volcanism and faulting since ~16.6 Ma has created a region optimal for field-based studies aimed at investigating factors controlling the formation and modification of continental lithosphere. The HVLM lies ~50 km north of the Nevada-Oregon border in a transitional location between the High Lava Plains and northwest Basin and Range provinces (Carlson and Hart, 1987; Colgan et al., 2006; Lerch et al., 2008). Additionally, the HVLM is in the western portion of the Idaho-Oregon-Nevada (ION) region that serves as the intersection of three mid-Miocene to Recent tectonomagmatic features; the NE-striking Snake River Plain-Yellowstone trend (SRP), the NW-striking High Lava Plains-Newberry trend (HLP), and the NNW-striking Northern Nevada Rift (Pierce and Morgan, 1992; Zoback et al., 1994; John et al., 2000; Jordan et al., 2004; Brueseke et al., 2008; Meigs et al., 2009). Mid-Miocene to Recent basaltic and bimodal basalt-rhyolite volcanism and extension in the northwestern United States is associated with processes related to convergence between the North American Plate and various oceanic plates and terranes coupled with the effects of the Yellowstone-Newberry thermal anomaly (e.g., Christiansen and Lipman, 1972; Carlson and Hart, 1987; Pierce and Morgan, 1992; Camp and Ross, 2004; Jordan et al., 2004; Pierce and Morgan, 2009). The exact causes and effects of the Yellowstone-Newberry thermal anomaly are not yet fully understood.

Following a brief magmatic hiatus (ca. 19-17 Ma) that marked a period of significant regional tectonic change, major outpourings of basaltic magma (Steens Mountain and Columbia River Basalts) initiated from vent locations extending for over 1000 km from SE Washington to central Nevada, and from isolated locations to the east and west (e.g., Carlson and Hart, 1987; Zoback et al., 1994; Camp and Ross, 2004). The development of compositionally diverse, although fundamentally bimodal volcanic fields and silicic dome (HVLM) and caldera complexes in the ION region was synchronous with or followed shortly after flood basalt activity (Brueseke et al., 2008 and references therein). ION area mid-Miocene silicic volcanism became distributed into opposing time-transgressive tracks (SRP and HLP) during the Late Miocene. In both cases the spatial-temporal progression is marked by initiation of silicic eruptive centers, with basaltic volcanism following and remaining locally active to the present-day. The HLP, a locus of basalt-rhyolite volcanism after 10 Ma, broadly coincides with the Brothers Fault Zone (e.g., Meigs et al., 2009 and references therein), which is a broad NW-striking zone of small en-echelon faults (Lawrence, 1976).

The northwest Basin and Range (NWBR) extends to the Cascade volcanic arc in the west and the HLP/Brothers Fault Zone in the north. Tectonic controls on the NWBR are influenced by Middle- to Late-Miocene development and northward propagation of the Walker Lane, a younger complement to the San Andreas transform system (e.g., Wesnousky, 2005). The Walker Lane transform system is likely influencing the NWBR by causing extension or counterclockwise block rotation at its western boundary (Pezzopane and Weldon, 1993; Faulds et al., 2005; Scarberry et al., 2010). Deformation south of the HLP is accommodated along faults that exhibit two principal strike directions: NNE and NW, as observed in the HVLM (Pezzopane and Weldon, 1993; Crider, 2001; Scarberry et al., 2010). NNE-striking, large offset (100's of meters) normal faults form the dominant topographic features of the landscape. Isolated zones of NW-striking, small offset (10's of meters) oblique-slip faults intersect and are overprinted by the NNE-striking Basin and Range fabric (e.g., Walker and MacLeod, 1991 and references therein). Structures within the NWBR formed after ~10 Ma and NW-striking faults may form in advance of NNE-striking Basin and Range faults in any particular location. Extension of the NWBR along NNE-striking Basin and Range style faults is believed to be minor compared with the central Basin and Range. For example a field-based structural study across Abert Rim located west of the HVLM map area indicates that NW-striking faults formed prior to the principal NNE-striking escarpment and that net extension since 16 Ma is on the order of ~3% (Scarberry et al., 2010), consistent with other recent regional estimates of <17-20% (e.g., Lerch et al., 2008).

Our new mapping at the 1:24,000 scale plus associated data, coupled with previous reconnaissance mapping and geochronologic and geochemical data (Legge, 1988; Pasquale and Hart, 2006; Tables 1-3) indicate that the HVLM is characterized by a NW-striking structural valley that cuts an ~150 km² 16.3±0.3 Ma, largely trachyte-rhyolite volcanic complex. Available radiometric ages and stratigraphic relationships indicate that the bulk of HVLM volcanism occurred during a <1 m.y. window synchronous with or shortly following eruption of the Steens Basalt from fissures in the Steens-Pueblo Mountains located less than 20 km to the east. Local HVLM eruptions produced small volumes of Quaternary basalt (0.6±0.3 Ma) that were erupted along and offset by reactivated NNE-striking structures. In contrast, NW-striking faults with rare exception displace only the mid-Miocene silicic lavas and are in turn cut by NNE-striking structures. Numerous rhyolite/trachyte vents are situated at or near the intersection of NNE- and NW-striking structures indicating that both structural trends were active and available for magma passage in the mid-Miocene. These vents produced physically, petrographically, and chemically distinct units. The observations and data suggest: 1) influx of regionally voluminous mantle-derived melts (Steens Basalt) starting at ~16.6 Ma provided the thermal and material inputs driving crustal modification and establishment of the HVLM silicic magmatic systems, 2) source (heterogeneous mantle and crustal melts) and process (fractional crystallization, assimilation, magma mixing) related factors are responsible for within and between vent/unit geochemical heterogeneity, 3) separate relatively small upper-level magmatic systems were established along regional lithospheric weaknesses, with their eruption likely triggered by periods of heightened regional/local tectonic or/and magmatic activity, and 4) following an ~15 m.y. hiatus, HVLM volcanism reinitiated with small volume basaltic eruptions from vents along active zones of NWBR deformation, with the basalt flow field subsequently displaced by NNE-striking normal faults.

Table 1: ^{40}Ar / ^{39}Ar Radiometric Age Determinations

Sample	Map # / Unit	Material	Plateau (Ma) Age ± 2 σ	Plateau (Ma) Steps	Plateau (Ma) %^{39}Ar	Plateau (Ma) MSWD	Normal Isochron (Ma) Age ± 2 σ	Normal Isochron (Ma) $^{40}Ar/^{36}Ar$ ± 2 σ	Total Fusion (Ma) Age ± 2 σ
PL-100	13 / Ttd2	feldspar	**16.40 ± 0.19**	8/11	97.0	1.98	16.36 ± 0.19	376.7 ± 43.4	16.40 ± 0.19
PL-162	14 / Ttd2	feldspar	**16.46 ± 0.21**	10/12	98.8	1.67	16.43 ± 0.22	316.3 ± 53.0	16.45 ± 0.21
SP04-10	19 / Tr1	feldspar	**16.51 ± 0.25**	8/11	71.2	0.32	16.52 ± 0.25	294.8 ± 6.3	16.64 ± 0.25
SP04-25	nom / Tr3	feldspar	**16.39 ± 0.17**	14/14	100.0	1.76	16.38 ± 0.18	304.2 ± 17.5	16.39 ± 0.17
SP04-32	32 / Tr4	feldspar	**16.33 ± 0.17**	12/12	100.0	2.18	16.36 ± 0.17	286.7 ± 19.8	16.33 ± 0.17

Plateau age data includes number of steps in the plateau (steps in plateau / total steps) and % ^{39}Ar in plateau. Samples not within map area indicated as nom.

Table 2: K/Ar Radiometric Age Determinations

Sample	Map # / Unit	Material	Age ± 2 σ	Weight (gm)	K_2O (wt%)	$^{40}Ar^*$ (m/gm)	$^{40}Ar^*$ (%)
PL-193	1 / Qb	whole-rock	**0.47 ± 0.23**	5.012	0.246	1.65×10^{-13}	0.83
PL-69	3 / Qb	whole-rock	**0.81 ± 0.25**	5.035	0.242	2.83×10^{-13}	1.18
PL-107C	nom / Tt2	whole-rock	**16.25 ± 0.26**	5.020	4.096	9.626×10^{-11}	80.7
PL-162	14 / Ttd2	whole-rock	**16.38 ± 0.26**	3.147	5.269	1.248×10^{-10}	85.9

Samples not within map area indicated as nom.

Table 3: Representative Chemical Analyses of Map Units

Sample	PL-193	PL-47B	PL-69	AW09-07	AW09-05	PL-41C	SP04-48	PL-107C	AW09-04	SP04-04	SP04-08	PL-79	PL-65	SP04-36	PL-79B	SP04-42	PL-76B	PL-50C	PL-136	SP04-40	PL-128	SP04-46	SP04-25	SP04-22
Map #	1	2	3	4	5	6	nom	nom	7	8	9	10	22	23	10	24	25	26	nom	nom	27	28	nom	29
Map Unit	Qb	Qb	Qb	Qb	Qb	Qb	Tt1	Tt2	Tt2	Tt3	Tt3	Ttd1	Tr1	Tr1	Tr1	Tr1	Tr1	Tr1	Tr2	Tr2	Tr2	Tr3	Tr3	Tr3
NLat(27)°	42.1299	42.1582	42.1779	42.1105	42.1532	42.1445	42.1202	42.2749	42.2038	42.0594	42.0686	42.1919	42.1669	42.1407	42.1919	42.1330	42.1902	42.1651	42.1443	42.1363	42.1390	42.0941	42.1039	42.0947
WLong(27)°	119.1120	119.0846	119.0644	119.1123	119.0497	119.0845	119.1325	118.9570	119.0372	119.0346	119.0441	119.0375	119.0600	119.0259	119.0375	119.0974	119.0610	119.0834	118.9742	118.9181	119.0048	119.1020	119.1320	119.1137
SiO_2 (wt%)	47.51	47.58	47.98	48.19	48.40	48.64	63.91	63.59	64.12	64.25	64.41	68.64	72.01	72.11	72.61	73.24	73.70	74.11	72.04	72.99	73.97	71.92	72.14	72.24
TiO_2	1.00	0.93	0.92	0.96	0.99	0.98	1.04	0.96	0.94	0.84	0.82	0.63	0.42	0.36	0.33	0.27	0.25	0.21	0.34	0.29	0.23	0.34	0.33	0.31
Al_2O_3	17.17	16.95	17.21	17.16	16.72	16.66	16.63	16.12	16.12	16.13	15.73	15.63	14.88	14.61	14.24	14.92	14.04	13.52	14.93	14.48	13.80	14.87	14.62	14.37
Fe_2O_3	3.63	3.66	3.46	3.53	3.43	3.52	2.66	2.96	2.75	2.50	2.52	1.82	1.43	1.35	1.22	0.95	1.05	0.95	1.19	1.18	1.14	1.25	1.16	1.19
FeO	7.27	7.21	7.05	7.09	6.68	6.88	2.48	2.77	2.49	2.24	2.20	1.51	1.13	1.04	0.95	0.77	0.80	0.73	0.86	0.85	0.80	0.87	0.78	0.78
MnO	0.19	0.18	0.18	0.19	0.18	0.18	0.08	0.10	0.11	0.13	0.12	0.11	0.04	0.07	0.04	0.03	0.06	0.04	0.05	0.08	0.04	0.07	0.07	0.06
MgO	9.22	9.35	9.52	8.74	8.47	8.64	0.95	1.61	1.41	1.58	1.69	0.38	0.16	0.26	0.24	0.15	0.13	0.11	0.06	0.07	0.03	0.06	0.11	0.06
CaO	10.96	10.99	10.92	11.27	12.07	11.44	3.52	3.19	3.17	3.35	3.26	1.87	0.84	1.10	1.18	0.68	0.85	1.13	0.48	0.26	0.33	0.40	0.44	0.40
Na_2O	2.63	2.81	2.39	2.55	2.67	2.67	4.59	4.40	4.32	4.27	3.67	4.56	4.20	4.43	4.34	3.74	3.51	4.17	4.61	4.41	4.44	4.76	4.72	4.69
K_2O	0.25	0.23	0.24	0.21	0.23	0.23	3.70	3.99	4.24	4.42	5.32	4.65	4.84	4.56	4.73	5.19	5.56	4.87	5.37	5.32	5.20	5.39	5.53	5.86
P_2O_5	0.16	0.11	0.13	0.10	0.16	0.16	0.45	0.32	0.33	0.29	0.27	0.20	0.03	0.13	0.12	0.07	0.05	0.17	0.07	0.07	0.03	0.06	0.09	0.04
Total	99.98	100.01	100.04	99.79	100.76	100.06	99.31	98.85	99.57	99.25	98.94	96.86	97.46	98.85	97.52	95.76	97.94	97.08	97.76	98.32	99.07	98.73	99.62	99.33
Rb (ppm)	6	13	13	7	5	7	103	148	109	117	121	141	167	182	174	172	200	169	167	184	188	169	164	169
Sr	252	241	255	196	226	213	418	323	306	287	258	224	100	147	118	73	94	70	47	21	15	26	28	27
Ba	134	120	139	166	110	143	1173	954	1026	1034	1024	1040	585	723	530	652	500	364	595	281	135	430	533	425
Zr	78	80	85	55	61	55	278	350	326	342	333	313	268	235	224	241	238	213	390	404	397	391	383	377
Nb	nd	nd	nd	nd	nd	nd	15	nd	8	16	16	17	29	37	23	23	nd	25	25	28	30	25	26	25
Y	25	30	31	24	24	23	41	61	30	43	34	40	40	24	30	26	44	31	47	42	43	47	58	47
Zn	nd	nd	nd	71	74	65	75	nd	87	75	64	78	51	56	48	37	nd	82	66	65	64	63	75	64
Ni	148	155	156	133	123	114	4	10	27	14	11	18	13	5	12	2	3	11	1	<1	1	1	1	<1
V	265	254	236	231	257	245	64	92	97	92	82	25	18	22	19	14	5	5	16	8	10	17	14	14
Sc	nd	nd	nd	34	37	36	11	nd	12	12	11	7	6	4	5	nd	5	5	5	4	6	6	7	**7**

Sample	AW09-15	PL-191	PL-113	PL-100	PL-162	SP04-20	PL-63	SP04-33	AW09-06	SP04-10	AW09-14	AW09-16	SP04-45	SP04-29	SP04-32	SP04-43	SP04-03	SP04-01	SP04-07	PL-184B	SP04-50	AW09-12	SP04-06
Map #	nom	11	12	13	14	15	16	17	18	19	20	21	30	31	32	33	34	35	36	37	nom	nom	38
Map Unit	Ttd1	Ttd2	Ttd2	Ttd2	Ttd2	Ttd2	Ttd2	Ttd2	Tr1	Tr1	Tr1	Tr1	Tr4	Tr4	Tr4	Tr4	Tr4	Tr4	Tr5	Twt1	Twt1	Twt1	Twt2
NLat(27)°	42.1635	42.0942	42.1357	42.1173	42.1131	42.1213	42.1125	42.1257	42.1853	42.1683	42.1659	42.1607	42.0902	42.0772	42.0742	42.1247	42.0576	42.0668	42.0656	42.0898	42.1167	42.0701	42.0650
WLong(27)°	118.9992	119.0360	119.0110	119.0186	119.0015	119.0099	119.0387	119.0498	119.0812	119.0846	119.0081	119.0134	119.0953	119.0768	119.1203	119.1046	119.0324	119.0307	119.0443	119.1116	119.1477	119.2437	119.0454
SiO_2 (wt%)	68.92	68.74	68.87	68.92	68.99	69.15	69.47	70.02	70.39	71.22	71.67	71.93	71.89	73.05	73.11	73.88	74.52	74.95	72.26	75.09	75.85	76.52	71.74
TiO_2	0.60	0.53	0.56	0.56	0.55	0.52	0.50	0.43	0.48	0.39	0.39	0.42	0.33	0.26	0.21	0.22	0.17	0.18	0.33	0.17	0.21	0.19	0.35
Al_2O_3	15.38	16.92	15.93	15.80	15.93	16.60	15.62	15.80	14.86	14.33	14.57	14.98	14.73	14.18	15.43	13.72	13.54	13.43	14.50	13.24	12.19	11.93	14.79
Fe_2O_3	1.73	1.63	1.63	1.67	1.61	1.56	1.50	1.33	1.50	1.41	1.34	1.52	1.30	1.03	1.12	1.11	0.93	0.71	1.14	1.08	1.24	1.15	1.13
FeO	1.45	1.24	1.23	1.28	1.23	1.23	1.12	0.99	1.27	1.11	1.03	1.22	0.94	0.75	0.97	0.76	0.62	0.46	0.79	0.75	0.85	0.82	0.83
MnO	0.07	0.06	0.05	0.06	0.06	0.04	0.05	0.07	0.09	0.08	0.06	0.03	0.08	0.10	0.09	0.07	0.08	0.02	0.07	0.06	0.07	0.07	0.10
MgO	0.60	0.17	0.25	0.22	0.28	0.18	0.22	0.20	0.62	0.53	0.24	0.16	0.18	0.12	0.14	0.06	0.04	0.02	0.20	0.00	0.09	0.07	0.25
CaO	1.96	0.73	1.10	1.22	1.19	0.69	0.96	0.89	1.64	1.45	1.36	0.76	0.69	0.56	0.44	0.18	0.16	0.11	0.70	0.13	0.03	0.09	0.81
Na_2O	4.11	4.54	4.74	4.69	4.68	4.15	4.65	4.65	3.92	3.54	4.41	4.03	4.70	4.05	3.24	4.45	4.87	4.75	4.59	4.48	4.38	4.35	4.17
K_2O	4.99	5.40	5.40	5.37	5.26	5.84	5.51	5.49	5.03	5.80	4.70	4.92	5.06	5.83	5.17	5.48	5.06	5.35	5.39	4.96	5.02	4.78	5.76
P_2O_5	0.19	0.02	0.24	0.20	0.22	0.04	0.39	0.13	0.18	0.14	0.23	0.03	0.09	0.06	0.07	0.07	0.01	0.01	0.03	0.02	0.07	0.02	0.06
Total	96.87	98.07	97.91	97.04	97.64	95.96	97.53	97.65	95.60	97.08	98.53	97.15	98.80	97.40	94.44	98.69	100.20	99.91	99.45	99.30	99.52	98.42	97.67
Rb (ppm)	148	130	146	148	151	153	150	153	167	172	165	159	163	179	178	195	203	211	177	223	188	194	182
Sr	202	114	181	174	158	120	138	113	165	159	150	100	69	46	20	9	11	10	63	11	10	8	67
Ba	842	1052	1395	1375	1185	1197	1240	1151	749	886	890	613	707	530	194	122	118	106	463	234	137	47	492
Zr	294	430	408	397	421	377	405	373	292	247	265	260	335	304	372	379	345	363	295	395	470	472	291
Nb	27	nd	22	21	22	22	22	22	24	31	23	29	25	28	36	31	33	33	26	nd	27	19	25
Y	34	23	28	31	36	32	26	36	37	33	39	30	46	47	98	85	54	66	47	42	47	51	45
Zn	52	nd	55	60	57	54	49	50	58	52	57	51	58	73	89	76	68	92	51	nd	84	82	61
Ni	17	3	3	2	2	3	2	2	11	1	10	12	1	<1	<1	<1	1	2	<1	3	<1	2	<1
V	25	10	28	29	30	26	25	22	27	28	18	25	14	8	9	11	7	4	17	<2	7	<2	15
Sc	7	nd	7	8	8	7	7	7	8	6	4	6	5	5	6	4	3	6	nd	6	6	7	

Major element data in weight (wt) % and trace element data in parts per million (ppm); major element data reported as 100% anhydrous after conversion of total Fe to FeO and Fe_2O_3 (LeMaitre, 1976) with pre-normalization total reported. Locations quoted for NAD27 datum. Abbreviations for samples not located within map boundary (nom) and element concentrations not determined (nd).

OPEN-FILE REPORT O-11-12

Geologic Map of the Hawks Valley-Lone Mountain Region, Harney County, Oregon
By Alicja Wypych, William K. Hart, Kaleb C. Scarberry, Kelly C. McHugh, Stephen A. Pasquale and Paul W. Legge

This geologic mapping was funded in part by the U.S. Geological Survey (EDMAP) Award No. G09AC00145
and the National Science Foundation (EAR) EAR-0506887

PLATE 1

NOTICE

This map cannot serve as a substitute for site-specific investigations by qualified practicioners. Site-specific data may give results that differ from those shown on the maps. The views and conclusions contained in this document are those of the authors and should not be interpreted as necessarily representing the official policies, either expressed or implied, of the U.S. government.

For further detailed geologic information, please refer to accompanying report.

METHODS

Samples for whole-rock chemical, K-Ar, and Ar-Ar analysis (Tables 1-3) were collected to minimize secondary alteration and were processed to minimize laboratory contamination. All samples were either cut into slabs on a water-cooled diamond saw or split into pieces with a hydraulic splitter followed by removal of alteration and metallic residue via a water-cooled silicon carbide belt sander, after which they were washed in deionized water and dried at room temperature. Material further processed for whole-rock geochemical analysis was done so via sequential size reduction to <0.15 mm via steel jaw crusher, alumina ceramic disc mill, and alumina ceramic shatterbox mill. Material further processed for geochronology was crushed in a steel mortar and pestle and/or steel jaw crusher to size fractions of ~0.5-1.7 mm (whole-rock K-Ar) or ~0.25-0.5 mm (Ar-Ar), washed in deionized water and dried at 40 °C for ~12 hours. For the Ar-Ar analyses, feldspars were isolated as a non-magnetic fraction at 2.0 ampres with a Frantz Magnetic Barrier Separator.

$^{40}Ar/^{39}Ar$ ages were obtained at Oregon State University (OSU) (Table 1). Samples were irradiated at the OSU TRIGA reactor for 7 hours at 1MW power, and the neutron flux was monitored using the FCT-3 biotite standard (28.03 Ma; Renne et al., 1994). Analyses were done with a Mass Analyzer Products MAP-215/50 operating in peak-hopping mode. Plateau ages were preferred for all samples. Details of the procedures used at Oregon State University are provided in Jordan et al. (2004). K-Ar ages (Table 2) were determined at Case Western Reserve University using a low volume extraction system coupled with a MS-10 mass spectrometer following the procedures outlined in Hart et al. (1984) and Hart and Carlson (1985). Decay constants used for Ar-Ar and K-Ar are those recommended by Steiger and Jäger (1977).

Major and trace element concentrations (Table 3) were determined by x-ray fluorescence spectrometry (XRF) at Franklin & Marshall College following the procedures outlined by Mertzman (2000) and/or by direct current argon plasma optical emission spectroscopy (DCP-OES) at Miami University following the procedures of Katoh et al. (1999) as described in Brueseke and Hart (2008).

REFERENCES

Brueseke, M.E. and Hart, W.K., 2008. Geology and petrology of the mid-Miocene Santa Rosa – Calico Volcanic Field, northern Nevada: Nev. Bur. Mines Geol. Bull., 113.
Brueseke, M.E., Hart, W.K., and Heizler, M.T., 2008. Diverse mid-Miocene silicic volcanism associated with the Yellowstone-Newberry thermal anomaly: Bull. Volcanol., 70: 343-360.
Camp, V. E., and Ross, M.E., 2004. Mantle dynamics and genesis of mafic magmatism in the intermountain Pacific Northwest: J. Geophys. Res., 109: B08204.
Carlson, R.W. and Hart, W.K., 1987. Crustal Genesis on the Oregon Plateau: J. Geophys. Res., 92: 6191-6206.
Castor, S.B. and Henry, C.D., 2000. Geology, geochemistry, and origin of volcanic rock-hosted uranium deposits in northwestern Nevada and southeastern Oregon, USA: Ore Geol. Rev., 16: 1-40.
Christiansen, R.L. and Lipman, P.W., 1972. Cenozoic volcanism and plate tectonic evolution of the western United States - Part II, Late Cenozoic: Phil. Trans. Roy. Soc. Lon., A271: 249-284.
Colgan, J.P., Dumitru, T.A., McWilliams, M., and Miller, E.L., 2006. Timing of Cenozoic volcanism and Basin and Range extension in northwestern Nevada: New constraints from the northern Pine Forest Range: Geol. Soc. Amer. Bull., 118: 126–139.
Crider, J.G., 2001. Oblique slip and the geometry of normal-fault linkage; mechanics and a case study from the Basin and Range in Oregon: J. Struct. Geol., 23: 1997-2009.
Faulds, J.E., Henry, C.D., and Hinz, N.H., 2005. Kinematics of the northern Walker Lane: incipient transform fault along the Pacific North American plate boundary: Geology, 33: 505-508.
Green, R.C., 1984. Geologic appraisal of the Charles Sheldon Wilderness Study Area, Nevada and Oregon: US Geol. Surv. Bull., 1538: 13–34.
Hart, W.K. and Carlson, R.W., 1985. Distribution and geochronology of Steens Mountain type basalt from the northwestern Great Basin: Isochron/West, 43: 5-10.
Hart, W.K., Aronson, J.L., and Mertzman, S.A., 1984. Aerial distribution and age of low-K, high-alumina olivine tholeiite magmatism in the northwestern Great Basin, U.S.A.: Geol. Soc. Amer. Bull., 95: 186-195.
Henry, C. D., Castor, S. B., McIntosh, W. C., Heizler, M. T., Cuney, M., and Chemillac, R., 2006. Timing of oldest Steens Basalt magmatism from precise dating of silicic volcanic rocks, McDermitt Caldera and Northwest Nevada volcanic field: Eos Transactions AGU 87 (52), Fall Meet. Suppl., V44C-08.
Jarboe, N.A., Coe, R.S., Renne, P.R., and Glen, J.M.G., 2010. The age of the Steens reversal and the Columbia River Basalt Group: Chem. Geol., 274: 158-168.
John, D.A., Wallace, A.R., Ponce, D.A., Fleck, R.L., and Conrad, J.E., 2000. New perspectives on the geology and origin of the Northern Nevada Rift, in Cluer, J.K., Price, J.G., Struhsacker, E.M., Hardyman, R.F., and Morris, C.L., (eds.), Geology and Ore Deposits 2000: The Great Basin and Beyond: Geol. Soc. Nev. Symp. Proc., 127-154.
Jordan, B.T., Grunder, A.L., Duncan, R.A., and Deino, A.L., 2004. Geochronology of Oregon High Lava Plains volcanism: Mirror image of the Yellowstone hotspot?: J. Geophys. Res., 109: B10202.
Katoh, S., Danhara, T., Hart, W.K., and WoldeGabriel, G., 1999. Use of sodium polytungstate solution in the purification of volcanic glass shards for bulk chemical analysis: Nat. and Human Act., 4: 45-54.
Lawrence, R.D., 1976. Strike-slip faulting terminates the Basin and Range province in Oregon: Geol. Soc. Amer. Bull., 87: 846-850.
Legge, P., 1988. The bimodal basalt-rhyolite association west of and adjacent to the Pueblo Mountains, southeastern Oregon: [M.S. thesis] Miami University.
LeMaitre, R.W., 1976. Some problems of the projection of chemical data into mineralogical classifications: Contrib. Mineral. Petrol., 56: 181-189.
Lerch, D.W., Miller, E.L., McWilliams, M., and Colgan, J.P., 2008. Tectonic and magmatic evolution of the northwestern Basin and Range and its transition to unextended volcanic plateaus: Black Rock Range, Nevada: Geol. Soc. Amer. Bull., 120: 300-311.
Meigs, A., Scarberry, K., Grunder, A., Carlson, R., Ford, M., Fouch, M., Grove, T., Hart, B., Iademarco, M., Jordan, B., Milliard, J., Streck, M., Trench, D., and Weldon, R., 2009. Geological and geophysical perspectives on the magmatic and tectonic development of the High Lava Plains and northwest Basin and Range, in Dorsey, R.J., Madin, I.P., and O'Connor, J.E., eds., Volcanoes to Vineyards: Geologic Field Trips through the Dynamic Landscape of the Pacific Northwest: Geol. Soc. Amer. Field Guide, 15: 435-470.
Mertzman, S.A., 2000. K-Ar results from the southern Oregon - northern California Cascade Range: Ore. Geol., 62: 99–122.
Pasquale, S. and Hart, W.K., 2006. The tectonomagmatic development of a mid-Miocene silicic eruptive center near the Oregon Plateau-Basin & Range boundary, SE Oregon: Geol. Soc. Amer. Abs. with Prog., 38: 94.
Pezzopane, S.K., and Weldon, R.J., 1993. Tectonic role of active faulting in central Oregon: Tectonics, 12: 1140-1169.
Pierce, K.L. and Morgan, L.A., 1992. The track of the Yellowstone hotspot; volcanism, faulting and uplift: Geol. Soc. Amer. Mem., 79: 1-53.
Pierce, K.L. and Morgan, L.A., 2009. Is the track of the Yellowstone hotspot driven by a deep mantle plume? — Review of volcanism, faulting, and uplift in light of new data: J. Volcanol. Gerotherm. Res., 188: 1–25.
Renne, P.R., Deino, A.L., Walter, R.C., Turrin, B.D., Swisher, C.C., Becker, T.A., Curtis, G.H., Sharp, W.D., and Jaouni, A.R., 1994. Intercalibration of astronomical and radioisotopic time: Geology, 22: 783-786.
Rytuba, J.J. and McKee, E.H., 1984. Peralkaline ash flow tuffs and calderas of the McDermitt volcanic field, southeast Oregon and north central Nevada: J. Geophys. Res., 89: 8616-8628.
Scarberry, K.C., Meigs, A.J., and Grunder, A.L., 2010. Faulting in a propagating continental rift: Insight from the late Miocene structural development of the Abert Rim fault, southern Oregon, USA: Tectonophys., 488: 71–86.
Steiger, R.H., and Jäger, E., 1977. Subcommission on geochronology: Convention on the use of decay constants in geo- and cosmochronology: Earth Planet. Sci. Lett., 36: 359-362.
Walker, G.W., and MacLeod, N.S., 1991. Geologic map of Oregon: U.S. Geol. Surv., Reston, VA.
Wesnousky, S.G., 2005. The San Andreas and Walker Lane fault systems, western North America: transpression, transtension, cumulative slip and the structural evolution of a major transform plate boundary: J. Struct. Geol., 27: 1505–1512.
Zoback, M.L., McKee, E.H., Blakely, R.J., and Thompson, G.A., 1994. The northern Nevada rift: Regional tectono-magmatic relations and middle Miocene stress direction: Geol. Soc. Amer. Bull., 106: 371-382.

MAP SYMBOLS

Contact - dashed where inferred
Fault - dashed where inferred, dotted where concealed; ball and bar on down thrown side
○ Silicic dome
+ Mafic vent
Silicic or mafic vent area
Basaltic fissure
•1 Analyzed sample location

For copies of this publication contact:
Nature of the Northwest Information Center
800 NE Oregon Street, #28, Suite 965
Portland, Oregon 97232
telephone (971) 673-2331
http://www.naturenw.org